Incorporating Mouse Genome
Mammalian Genome
Genes and Phenotypes

Three ENU-induced neurological mutations in the pore loop of sodium channel *Scn8a* ($Na_v1.6$) and a genetically linked retinal mutation, *rd13*

David A. Buchner,[1,*] Kevin L. Seburn,[2,*] Wayne N. Frankel,[2] Miriam H. Meisler[1]

[1]Department of Human Genetics, University of Michigan, 4708 Medical Science II, Ann Arbor, Michigan, 48109-0618, USA
[2]The Jackson Laboratory, Bar Harbor, Maine, 04609, USA

Received: 22 September 2003 / Accepted: 2 December 2003

Abstract

The goal of The Jackson Laboratory Neuroscience Mutagenesis Facility is to generate mouse models of human neurological disease. We describe three new models obtained from a three-generation screen for recessive mutations. Homozygous mutant mice from lines *nmf2* and *nmf5* exhibit hind limb paralysis and juvenile lethality. Homozygous *nmf58* mice exhibit a less severe movement disorder that includes sustained dystonic postures. The mutations were mapped to the distal region of mouse Chromosome (Chr) 15. Failure to complement a mutant allele of a positional candidate gene, *Scn8a*, demonstrated that the mutations are new alleles of *Scn8a*. Missense mutations of evolutionarily conserved residues of the sodium channel were identified in the three lines, with the predicted amino acid substitutions N1370T, I1392F, and L1404H. These residues are located within the pore loop of domain 3 of sodium channel $Na_v1.6$. The lethal phenotypes suggest that the new alleles encode proteins with partial or complete loss of function. Several human disorders are caused by mutation in the pore loop of domain 3 of paralogous sodium channel genes. Line *nmf5* contains a second, independent mutation in the *rd13* locus that causes a reduction in cell number in the outer nuclear layer of the retina. *rd13* was mapped to the distal 4 Mb of Chr 15. No coding or splice site mutations were detected in *Pde1b*, a candidate gene for *rd13*. The generation of three independent *Scn8a* mutations among 1100 tested G3 families demonstrates that the *Scn8a* locus is highly susceptible to ENU mutagenesis. The new alleles of *Scn8a* will be valuable for analysis of sodium channel physiology and disease.

Of the estimated 30,000 genes in the human genome, ≥99% are also present in the mouse genome (Mouse Genome Sequencing Consortium 2002). To generate mutant alleles that will provide insight into the function of each of these genes, large-scale ENU mutagenesis programs have been initiated at several centers around the world (Balling 2001; Williams et al. 2003). These programs have already generated many new models of human disease (Thaung et al. 2002; Kile et al. 2003). One new ENU-induced deafness mutant led to isolation of the human deafness gene DFNA36 (Vreugde et al. 2002). We now describe three new neurological mutants from The Jackson Laboratory mutagenesis program that have mutations in the voltage-gated sodium channel gene *Scn8a*.

The ten paralogous voltage-gated sodium channel genes in the mammalian genome differ with respect to tissue specificity, subcellular localization, and kinetic properties (Meisler et al. 2001a, 2001b; Yu and Catterall 2003). The channels contain four homologous domains, each with six transmembrane segments (Catterall 2000). The extracellular loop between transmembrane segments 5 and 6 of each domain re-enters the membrane to form the outer pore of the channel. This pore is essential for ion selectivity and voltage gating (Guy and Durrell 1995; Yamagishi et al. 2001; Hilber et al. 2001).

The sodium channel $Na_v1.6$, encoded by the gene *Scn8a*, is expressed in neurons throughout the central and peripheral nervous systems (Burgess et al. 1995; Schaller et al. 1995). $Na_v1.6$ is localized

*These authors contributed equally.

Correspondence to: M. H. Meisler, E-mail: meislerm@umich. edu

 DOI: 10.1007/s00335-004-2332-1 • Volume 15, 344–351 (2004) •

at the nodes of Ranvier in myelinated axons, at the initial segment in retinal ganglion cells and Purkinje cells, and in the axons and dendrites of unmyelinated neurons (Caldwell et al. 2000; Jenkins and Bennett 2001; Black et al. 2002; Boiko et al. 2003). Mutations of *Scn8a* are responsible for several inherited neurological disorders in the mouse (Meisler et al. 2001a). The *Scn8a* null phenotype includes ataxia, tremor, and progressive paralysis with juvenile lethality at 3 weeks of age. The age at lethality corresponds to the final stage of developmental replacement of sodium channel $Na_v1.2$ at immature nodes of Ranvier by $Na_v1.6$, the major channel at mature nodes (Boiko et al. 2001). Paralysis in *Scn8a* null mice is the result of impaired nerve conduction and reduced neurotransmitter release at the neuromuscular junction. Electrophysiological recordings from mutant mice demonstrated the role of $Na_v1.6$ in repetitive firing of cerebellar Purkinje cells and generation of resurgent sodium currents (Raman et al. 1997; Maurice et al. 2001; Khaliq et al. 2003). The hypomorphic allele $Scn8a^{medJ}$ produces 10% of normal levels of $Na_v1.6$, resulting in reduced nerve conduction velocity and a dystonic phenotype (Sprunger et al. 1999; Kearney et al. 2002). A modifier gene that affects splicing of the $Scn8a^{medJ}$ transcript was recently identified (Buchner et al. 2003). The new mutant alleles of *Scn8a* described here will further our understanding of the biophysical properties of voltage-gated sodium channels and the phenotypic consequences of impaired function.

Materials and Methods

Mice. Mice were generated at the JAX Neuroscience Mutagenesis Facility (http://nmf.jax.org). C57BL/6J mice were mutagenized with ethylnitrosourea (ENU) administered in three weekly injections of 80 mg/kg. G3 offspring were bred by using a three-generation backcross mating scheme (Justice 2000; Herron et al. 2002). Mice from lines *nmf2* (MGI Accession ID: 2183462), *nmf5* (MGI: 2183472), and *nmf58* (MGI: 2429910) are available from The Jackson Laboratory. Retinal morphology was analyzed in *Scn8a* null mice homozygous for the transgene-induced allele $Scn8a^{TgNA4Bs}$ (Burgess et al. 1995).

Genetic mapping. A Cartesian Microsys (Genomic Solutions, Ann Arbor, Mich.) was used to set up PCR reactions with fluorescence-labeled primer pairs corresponding to microsatellite markers (MWG Biotech AG, UK). PCR reactions were performed on an MJ Tetrad PCR machine or an Applied Biosystems 9700, and the products were analyzed by capillary electrophoresis with an Applied Biosystems 3700. Map distance and gene order was determined with the computer program MAPMAKER (Lander et al. 1987).

Preparation of DNA and RNA. Genomic DNA was prepared from brain by proteinase K digestion, phenol chloroform extraction, and ethanol precipitation. Total RNA was prepared from brain and converted to first-strand cDNA as described (Ji et al. 2001).

Sequence analysis. The *Scn8a* cDNA was amplified in eight overlapping fragments (primer sequences available on request). Exon 19 was amplified from genomic DNA with the forward primer 5′ TTCAG CATCA TGGGC GTTAA CCTG 3′ and the reverse primer 5′ GAACC CCGAG AGTGA TCCTG ATCT 3′. RT-PCR products were gel purified with the QIAquick Gel Extraction Kit (Qiagen, Valencia, CA). Both strands were sequenced on the ABI Model 3700 automated sequencer (University of Michigan Sequencing Core, R. Lyons, Director). DNA sequences were assembled with Sequencher 4.1 software (Gene Codes, Ann Arbor, Mich.).

Electrode implantation and EEG measurements. Two homozygous *nmf58* mice, approximately 3 months of age, were anesthetized with tribromoethanol (Avertin, 500 mg/kg i.p.) and placed in a stereotaxic holder fitted with a mouse incisor bar. Burr holes were drilled bilaterally, approximately 1 mm posterior to bregma, 1 mm lateral to midline, and two Teflon-coasted bipolar electrodes were implanted into the cerebral cortex at a depth of approximately 0.1–0.5 mm. Dental cement was used to hold the implant in place, and screws were placed at the periphery of the skull to anchor the cement. At least 24 h after surgery, EEG recordings were taken on live, freely moving mice. Recordings were made on two separate days for at least 2 h each, with a Grass EEG Model 12 Neurodata Acquisition System and PolyviewPro software.

Results

Neuromuscular phenotype in lines nmf2, nmf5, and nmf58. In order to detect ENU-induced, recessively inherited phenotypes, we generated third-generation (G3) offspring from mutagenized male mice (Herron et al. 2002). Six of the 34 G3 offspring of male *nmf5* developed bilateral hindlimb paralysis at between 2 and 3 weeks of age, with onset at 16 ± 2 days (n = 12). A similar phenotype was observed in 8/23 offspring of *nmf2* (onset at 16 ± 2d, n = 12), and 6/25 offspring of *nmf58* (onset at 20 ± 3d, n = 20). No

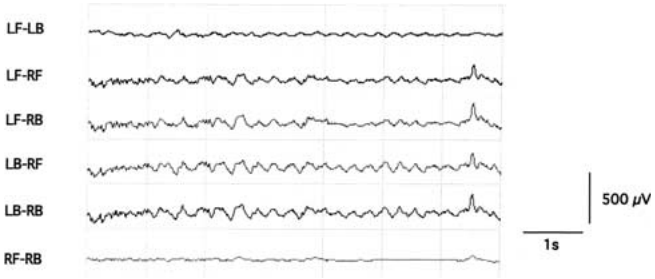

Fig. 1. Normal EEG recordings from affected mice in line *nmf58*. The six traces represent differential signals between four different electrodes. Most recordings showed no evidence of seizure activity. The one recorded spike was associated with a muscular twitch. Electrode positions are described in Methods. L, left; R, right; F, front; B, back.

abnormalities were detected in heterozygotes from all three lines. Deterioration of affected mice in lines *nmf2* and *nmf5* was rapid, and affected mice rarely survived to weaning at 3–4 weeks of age. Pathological examination of the peripheral nervous system, skeletal musculature, and neuromuscular junctions in strains *nmf2* and *nmf5* did not detect morphological defects. Affected mice in line *nmf58* appear more healthy, and some have survived to 3 months of age. The *nmf58* mice exhibit dystonic postures with twisting of the trunk and limbs that closely resemble the phenotype of mice carrying the hypomorphic allele Scn8amedJ (Sprunger et al. 1999).

In *nmf58* mice, muscle atrophy and regeneration of muscle fibers in the hindlimb were revealed by the presence of central nuclei at 45 days of age (data available online at http://nmf.jax.org/phenodev/NMF58cen%26rowing.html). These abnormalities were previously seen in mice carrying the hypomorphic allele $Scn8a^{medJ}$ (Sprunger et al. 1999). Muscle abnormalities were not observed in *nmf2* mice (n = 4) or *nmf5* mice (n = 8) analyzed at a younger age.

To determine whether the neurological phenotype included epileptic activity, we carried out EEG analysis. Two *nmf58* mutant mice that had survived for 3 months were recorded from implanted electrodes for >4 h on two different days. The EEG traces of both mice were generally normal, with no obvious signs of spike-wave discharges or other epileptic activity (Fig. 1). The occasional, isolated spikes were usually associated with a visible muscle twitch and are unlikely to reflect seizure activity.

Genetic mapping of recessive mutations. To map the *nmf5* mutation, the founder was outcrossed to strain BALB/cByJ, and the F_1 heterozygotes were intercrossed to generate F_2 progeny. A genome scan was carried out on pooled DNA from 20 affected and 20 unaffected F_2 mice. Linkage was confirmed by genotyping individual mice. *nmf5* was mapped to distal Chr 15 by linkage to microsatellite markers *D15Mit43* (LOD = 12.4) and *D15Mit35* (LOD = 8.1). The gene order and observed recombination fractions were: *D15Mit43*–(1/80)–*nmf5*–(3/80)–*D15Mit35*. The mutations in lines *nmf2* and *nmf58* were also mapped to distal Chr 15. For *nmf2*, the observed gene order was: *D15Mit171*–(13/80)–*nmf2*–(8/80)–*D15Mit35*. For *nmf58*, the gene order was: *D15Mit242*–(5/72)–*nmf58*–(2/72)–*D15Mit79*.

Complementation test with Scn8a. The position of the candidate gene *Scn8a* at 63 cM on distal mouse Chr 15 is within the overlapping nonrecombinant regions for the three new mutations. We therefore carried out a complementation test by crossing unaffected *nmf5* heterozygous carriers with $Scn8a^{medJ/+}$ heterozygotes. Seven of the 25 offspring were affected with the paralytic phenotype, in agreement with the prediction of 25% affected for a cross between allelic heterozygotes. Affected offspring were also obtained from crosses between *nmf5* heterozygotes and heterozygotes from lines *nmf2* (2/13) and *nmf58* (1/14). The failure to complement, together with the linkage data, indicates that lines *nmf2*, *nmf5*, and *nmf58* carry new mutant alleles of *Scn8a*.

Identification of missense mutations in Scn8a. The 6-kb coding region of the *Scn8a* cDNA was amplified by RT-PCR of brain RNA from homozygous affected individuals of the three strains. In addition, the alternatively spliced exons 5, 10, and 18 were amplified from genomic DNA. Both strands of the PCR products were sequenced and compared with genomic sequence from the background strain C57BL/6J (Mouse Genome Sequencing Consortium 2002). The cDNA from line *nmf2* contained an A → C substitution predicted to change asparagine 1370 to threonine (Fig. 2A). The cDNA from *nmf5* contained an A → T substitution changing isoleucine 1392 to phenylalanine (Fig. 2B). The cDNA from *nmf58* contained a T → A substitution changing leucine 1404 to histidine (Fig. 2C). The mutations were identified in RT-PCR products and confirmed by amplification and sequencing of exon 19 from genomic DNA (not shown). All three mutations are located in exon 19, which encodes the S5-S6 pore loop of domain 3 (Fig. 3 A). The alleles in lines *nmf2*, *nmf5*, and *nmf58* are designated $Scn8a^{N1370T}$, $Scn8a^{I1392F}$, and $Scn8a^{L1404H}$ respectively.

Retinal abnormalities in nmf5 mice. In the course of routine histological screening, a retinal

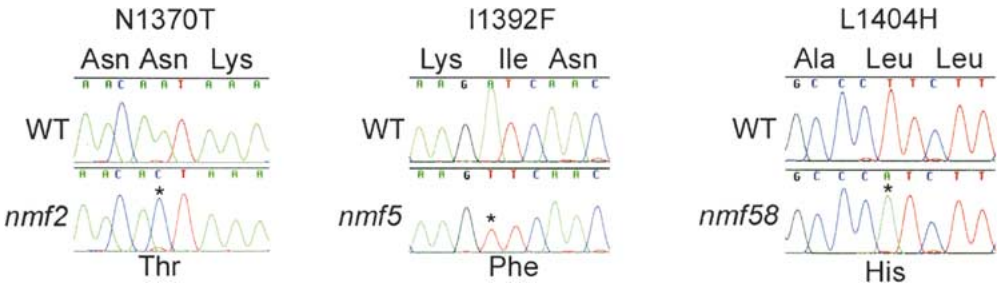

Fig. 2. Identification of ENU-induced mutations in the sodium channel $Na_v1.6$ (*Scn8a*). Sequence chromatograms for RT-PCR products from brain RNA. Mutations were confirmed in PCR products from genomic DNA (not shown).

abnormality was detected in *nmf5* mice affected with the neurological disorder. The outer nuclear layer of the retina of *nmf5* mice contains two to three layers of cells, rather than the 10–12 cell layers of normal retina (Fig. 4B,C). Cell loss did not appear to be progressive between 12 and 40 days of age. The effect of *Scn8a* mutations on retinal morphology has not been previously examined. To determine whether a null mutation of *Scn8a* results in abnormal development of the outer nuclear layer, we examined the retina of mice homozygous for the transgene-induced null allele, $Scn8a^{Tg}$ (Burgess et al. 1995). The retina of the $Scn8a^{Tg/Tg}$ mice was morphologically normal (Fig. 4A). This result suggested that *nmf5* mice carry a second mutation, linked to *Scn8a*, that is responsible for the retinal disorder.

To test this hypothesis, we examined F_2 progeny from a cross between line *nmf5* and strain A.B6-Tyr^+. One recombinant between the *Scn8a* mutation and the distal marker *D15Mit246* was obtained among 19 F_2 mice. The genotype of the recombinant individual was $D15Mit43^{A/B}$, $Scn8a^{I1392F/+}$, and $D15Mit246^{B/B}$. The recombinant displayed the retinal pathology but not the neurological phenotype. These data indicate that the retinal abnormality is caused by mutation of a distinct locus, designated *rd13*, with gene order *D15Mit43–Scn8a–D15Mit246*, *rd13*. Since *Scn8a* is located 4 Mb from the distal end of Chr 15, *rd13* must be located within this interval.

Evaluation of Pde1b as a candidate gene for rd13. The *Pde1b* gene encoding a β-subunit of rod phosphodiesterase is located within the target interval, approximately 3 Mb distal to *Scn8a* (Ensembl v15.3.1). The paralogous gene *Pde6b* is responsible for the classical retinal degeneration mutation on Chr 5, now designated *rd10*, which exhibits cell loss in the outer nuclear layer that is very similar to the *rd13* phenotype (Pittler and Baehr 1991). To test *Pde1b* as a candidate, we amplified the cDNA from brain of homozygous *nmf5* mice by RT-PCR. The products did not differ in size or sequence from the corresponding fragments amplified from C57BL/6J mice (data not shown). To confirm this result, we amplified each of the coding exons from genomic DNA of an affected *rd13* homozygote. There were no differences from wild-type sequence in the exons or adjacent sequences. The results indicate that *rd13* mice do not carry a coding or splice site mutation in *Pde1b*. Transcript levels were not quantitated, but the yield of RT-PCR products did not appear to be reduced in the mutant.

Discussion

We have identified three missense mutations of *Scn8a* that were induced by ENU mutagenesis. Previously studied null alleles of *Scn8a* result in hindlimb paralysis and lethality around 3 weeks of age, owing to the absence of $Na_v1.6$ from nodes of Ranvier in myelinated axons (Meisler et al. 1997). The hindlimb paralysis and juvenile lethality of affected mice in lines *nmf2* and *nmf5* suggest that these mutations are loss-of-function alleles The longer survival, muscle regeneration and dystonia observed in line *nmf58* resemble the hypomorphic allele $Scn8a^{medJ}$ (Sprunger et al. 1999). The new mutant alleles of *Scn8a* identify three residues in the pore loop of domain 3 that are critical for *in vivo* sodium channel function: N1370, I1392, and L1404. On the basis of site-directed mutagenesis and computer modeling, residue L1404 appears to be located within the pore helix but inaccessible from within the pore, while N1370 and I1392 contribute to the structure of the outer pore (Lipkind and Fozzard 2000; Yamagishi et al. 2001). The severe phenotypes of the new alleles support previous evidence that regions located immediately outside the membrane are essential for maintaining overall pore structure (Lipkind and Fozzard 2000). In the vertebrate sodium channel gene family, L1404 and N1370 are invariant residues, while residue 1392 is restricted to isoleucine or valine (Fig. 2B). Thus, all of these phenotypically severe mutants are nonconservative substitutions of evolutionarily conserved amino acid residues.

A minimal sodium channel containing only the S5 transmembrane segment, pore loop, and S6 segment, partially recapitulates the ion permeability of

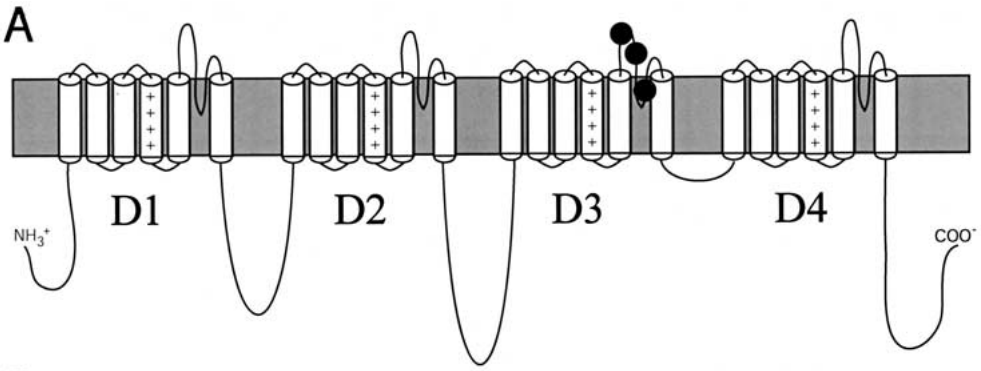

B

		nmf2				nmf5			nmf58	
		T				F			H	
SCN8A	DVN	N	KTECEKLMEGN-NTEIRWKNVK	I	NFDNVGAGYLA	L	LQVA
SCN2A	V..	.	YS..KA.I.S.Q.--A.....	V	.....L...S	.	....
SCN3A	...	.	LSD.QA..KQA-----.....	V	.....	.	....
SCN10A	I..	.	.SD.KIQNST---GSFF.V...	V	.....AM....	.	....
SCN11A	S.I	.	Y.IITNKSQCESGNF-S.I.Q.	V	.....NA...	.	....
SCN9A	Q.P	.	RS..FA..N-V-SQNV....L.	V	.....L...S	.	....
SCN4A	E..	.	.S...S..HTG---QV..L...	V	.Y....L...S	.	....
SCN5A	I..	.	.SQ..S.NLTG---.LY.TK..	V	.....	.	....
SCN1A	...	.	H.D.L..I.-R-.ETA.....	V	.....F...S	.	....
Fugu	V..	.	.SD.VA.Q.ATQ--.A..V...	V	.Y...AK...S	.	....
Eel	E..	.	RSD.MA..YT.---.V..V.L.	V	.Y..A.M...S	.	....
Squid	E..	.	RS...ENP--ML---YK...SP	.	.....LN....	.	F...
Flatworm	I..	S	.IA..TFANQLN---.T.I.S.	.	H..D.VN.L..	.	F...
Drosophila	IP.	R	NA-..SEN-------YT.V.SA	M	...H..NA..C	.	F...
Cockroach	IPD	R	NA-.IAEN-------YT.E.SP	M	...H..KA..C	.	F...
Jellyfish	VID	.	MAM.LNETNKAK.--YS.V.KN	.	....SIN.F..	.	F.T.

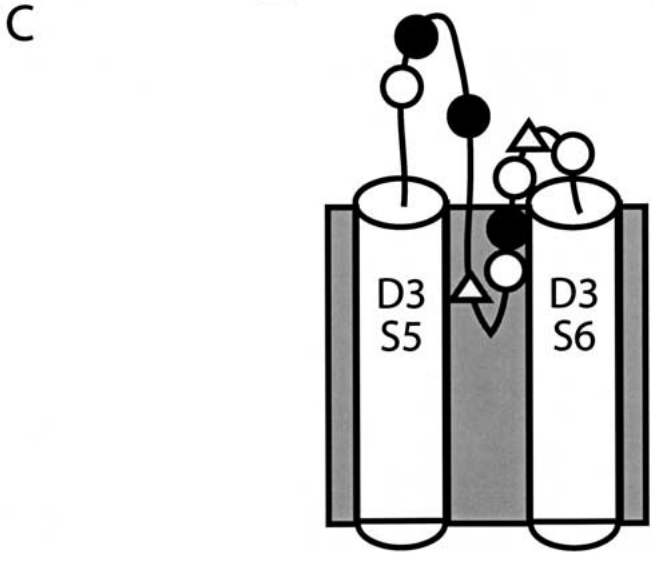

Fig. 3. Location of ENU-induced mutations in $Na_v1.6$. (**A**) The mutations in *nmf2*, *nmf5*, and *nmf58* mice are located in the pore loop of domain 3. (**B**) Evolutionary conservation of the D3 pore loop. The sequences of human SCN1A-11A are indicated. GenBank accession numbers, from top to bottom, are AF225988, AF327224, NM_006922, NM_006514, AF188679, NM_002977, NM_000334, AY038064, AB098335, AB030482, M22252, L19979, U93074, M32078, U73584, and AF047380. (**C**) Disease mutations in the D3 pore loop of related sodium channel genes. Open circle, human *SCN1A*; triangle, human *SCN5A*; closed circle, mouse *Scn8a*. Data from Ohmori et al. (2003), Sugawara et al. (2001), Kyndt et al. (2001), Deschenes et al. (2000) and this paper.

the intact channel (Chen et al. 2002). Missense mutations in the corresponding S5-S6 pore loop of sodium channels *SCN1A* and SCN5A have been identified in human patients with inherited epilepsy and cardiac disease, respectively (Fig. 2C). Functional analysis indicated that the patient mutations generate little or no sodium current (Deschenes et al. 2000; Kyndt et al. 2001; Sugawara et al. 2003). The best characterized mutation is G1406R in the cardiac channel *SCN5A* (Kyndt et al. 2001). Residue

Fig. 4. Reduced cell number in the retinal outer nuclear layer in *nmf5* mice. (**A**) *Scn8a*$^{-/-}$ null, (**B**) wildtype, (**C**) *nmf5*. ONL, outer nuclear layer; INL, inner nuclear layer.

G1406 of *SCN5A* corresponds to residue 1398 of *Scn8a*, which is located between the *nmf5* and *nmf58* mutations (Fig. 2B). G1406R does not affect protein stability or localization, but appears to inactivate the channel, since expression in a mammalian cell line did not generate detectable sodium current (Kyndt et al. 2001). It is likely that the ENU-induced mutations in *Scn8a* also encode proteins with reduced channel activity. Null alleles of the paralogous human gene *SCN1A* are associated with severe seizures in heterozygotes (Meisler et al. 2001b). We did not observe visible seizures in homozygotes for the *Scn8a* mutation in line *nmf58*, and the EEG recordings were normal (Fig. 1), suggesting that mutations in *Scn8a* are not associated with epilepsy. Normal EEGs have also been described in mice homozygous for the hypomorphic allele *Scn8a*^{medJ} (Hamann et al. 2003).

The low cell number in the outer nuclear layer of the retina in *nmf5* mice is the result of mutation of a novel locus, *rd13*, located distal to *Scn8a*. It is unclear whether the cell deficit in *rd13* mice is the result of a developmental defect or early onset degeneration. The early retinal degeneration (*erd*) mutation in the dog, with cellular phenotype and age of onset similar to *rd13*, has been mapped to the orthologous region of canine Chr 27 (Acland et al. 1999; Breen et al. 2001). A human retinal disorder has not been mapped to the corresponding region of human Chr 12q13. We tested *Pde1b* as a candidate gene for *rd13* because of its chromosome location and the fact that mutations in related phosphodiesterase subunits are responsible for retinal degeneration disorders in human and mouse (Pittman and Baehr 1991). No coding mutations or abnormal splice products were observed, but the possibility of altered regulation of *Pde1b* was not ruled out. When it is identified, the gene responsible for *rd13* will be an excellent candidate for canine *erd* and human autosomal recessive retinitis pigmentosa.

The per locus rate of ENU-induced mutations in *Scn8a*, 3/1100 G3 families, or 1/367, is at the high end of the previously reported range, 1/750 to 1/10,000 (Rinchik and Carpenter 1999). Other genes with multiple ENU-induced mutations are *Pde6b* (7/6500), *Pax6* (4/6500), and *Myo7a* (7/4557) (Thaung et al. 2002; Rinchik and Carpenter 1999). It is striking that three of the first 20 neurological mutants identified at the Neuroscience Mutagenesis Facility affect a single gene, especially since mutations in 289 different mouse loci have been associated with visible movement disorders (Blake et al. 2003). The clustering of these mutations in exon 19 of *Scn8a* is also unexpected, since disease mutations in human sodium channel genes are evenly distributed throughout the protein (Kohling 2002). It may be relevant that the *Scn8a* mutations arose on strain C57BL/6J, which could be predisposed to certain neurological phenotypes. C57BL/6J mice carry a defective allele of a putative splice factor that affects splicing of the *Scn8a* pre-mRNA, and this may influence susceptiblity to novel mutations (Buchner et al. 2003). As more ENU-induced mutations are identified, the molecular basis for variation in per locus mutation rates may become clear.

Acknowledgments

We acknowledge the contributions of Louise Dionne for recognition of the mutant phenotypes in lines *nmf2*, *nmf5*, and *nmf58*; Gregory Cox for advice on complementation testing; Joseph Brzezinski for assistance with retinal histology; and Maja Adamska for genomic sequencing of *Pde1b*. This work was supported by the Neuroscience Mutagenesis Facility at The Jackson Laboratory

(U01 NS41215), the Cancer Center Support Grant to The Jackson Laboratory (CA34196), and research grant R01 NS34509 (M.H. Meisler). D.A. Buchner acknowledges support from the Hearing and Chemical Senses Training Program (T32 DC00011). Genotyping was provided by The Jackson Laboratory Allele Typing Service.

References

1. Acland GM, Ray K, Mellersh CS, Langston AA, Rine J et al. (1999) A novel retinal degeration locus identified by linkage and comparative mapping of canine early retinal generation. Genomics 59, 134–142
2. Balling R (2001) ENU mutagenesis: analyzing gene function in mice. Annu Rev Genomics Hum Genet 2, 463–492
3. Black JA, Renganathan M, Waxman SG (2002) Sodium channel $Na_v1.6$ is expressed along nonmyelinated axons and it contributes to conduction. Brain Res Mol Brain Res 105, 19–28
4. Blake JA, Richardson JE, Bult CJ, Kadin JA, Eppig JT, Mouse Genome Database Group (2003) MGD: the Mouse Genome Database. Nucleic Acids Res 31, 193–195
5. Boiko T, Rasband MN, Levinson SR, Caldwell JH, Mandel G et al. (2001) Compact myelin dictates the differential targeting of two sodium channel isoforms in the same axon. Neuron 30, 91–104
6. Boiko T, Van Wart A, Caldwell JH, Levinson SR, Trimmer JS et al. (2003) Function specialization of the axon initial segment by isoform-specific sodium channel targetting. J Neurosci 23, 2306–2313
7. Breen M, Jouquand S, Renier C, Mellersh CS, Hitte C et al. (2001) Chromosome-specific single-locus FISH probes allow anchorage of an 1800-marker integrated radiation-hybrid/linkage map of the domestic dog genome to all chromosomes. Genome Res 11, 1784–1795
8. Buchner DA, Trudeau M, Meisler MH (2003) Scnm1, a putative RNA splicing factor that modifies disease severity in mice. Science 301, 967–969
9. Burgess DL, Kohrman DC, Galt J, Plummer NW, Jones JM et al. (1995) Mutation of a new sodium channel gene, *Scn8a*, in the mouse mutant 'motor endplate disease'. Nat Genet 10, 461–465
10. Caldwell JH, Schaller KL, Lasher RS, Peles E, Levinson SR (2000) Sodium channel Na(v)1.6 is localized at nodes of ranvier, dendrites, and synapses, Proc Natl Acad Sci USA 97, 5616–5620
11. Catterall WA (2000) From ionic currents to molecular mechanisms: the structure and function of voltage-gated sodium channels. Neuron 26, 13–25
12. Chen Z, Alcayaga C, Suarez-Isla BA, O'Rourke B, Tomaselli G et al. (2002) A ''minimal'' sodium channel construct consisting of ligated S5-P-S6 segments forms a toxin-activatable ionophore. J Biol Chem 277, 24653–24658
13. Deschenes I, Baroudi G, Berthet M, Barde I, Chalvidan T et al. (2000) Electrophysiological characterization of SCN5A mutations causing long QT (E1784K) and Brugada (R1512 W and R1432G) syndromes. Cardiovasc Res 46, 55–65
14. Guy HR, Durrell SR (1995) Structural models of Na+, Ca2+, and K+ channels. Soc Gen Physiol Ser 50, 1–16
15. Hamann M, Meisler MH, Richter A (2003) Motor disturbances in mice with deficiency of the sodium channel gene Scn8a show features of human dystonia. Exp Neurol 23, 184: 830–838
16. Herron BJ, Lu W, Rao C, Liu S, Peters H et al. (2002) Efficient generation and mapping of recessive developmental mutations using ENU mutagenesis. Nat Genet 30, 185–189
17. Hilber K, Sandtner W, Kudlacek O, Glaaser IW, Weisz E et al. (2001) The selectivity filter of the voltage-gated sodium channel is involved in channel activation. J Biol Chem 276, 27831–27839
18. Jenkins SM, Bennett V (2001) Ankyrin-G coordinates assembly of the spectrin-based membrane skeleton, voltage-gated sodium channels, and L1 CAMs at Purkinje neuron initial segments. J Cell Biol 155, 739–746
19. Ji W, Chen F, Do T, Do A, Roe BA et al. (2001) DQX1, an RNA-dependent ATPase homolog with a novel DEAQ box: expression pattern and genomic sequence comparison of the human and mouse genes. Mamm Genome 12, 456–461
20. Justice MJ (2000) Capitalizing on large-scale mouse mutagenesis screens. Nat Rev Genet 1, 109–115
21. Kearney JA, Buchner DA, De Haan G, Adamska M, Levin SI et al. (2002) Molecular and pathological effects of a modifier gene on deficiency of the sodium channel *Scn8a* ($Na_v1.6$). Hum Mol Genet 11, 2765–2775
22. Khaliq ZM, Gouwens NW, Raman IM (2003) The contribution of resurgent sodium current to high-frequency firing in Purkinje neurons: an experimental modeling sodium. J Neurosci 23, 4899–4912
23. Kile BT, Hentges KE, Clark AT, Nakamura H, Salinger AP et al. (2003) Functional genetic analysis of mouse chromosome 11. Nature 425, 81–86
24. Kohling R (2002) Voltage-gated sodium channels in epilepsy. Epilepsia 43, 1278–1295
25. Kyndt F, Probst V, Potet F, Demolombe S, Chevallier JC et al. (2001) Novel *SCN5A* mutation leading either to isolated cardiac conduction defect or Brugada syndrome in a large French family. Circulation 104, 3081–3086
26. Lander ES, Green P, Abrahamson J, Barlow A, Daly MJ et al. (1987) MAPMAKER: an interactive computer package for constructing primary genetic linkage maps of experimental and natural populations. Genomics 1, 174–181
27. Lipkind GM, Fozzard HA (2000) KcsA crystal structure as framework for a molecular model of the Na(+) channel pore. Biochemistry 39, 8161–8170
28. Maurice N, Tkatch T, Meisler M, Sprunger LK, Surmeier DJ (2001) D_1/D_5 Dopamine receptor activation differentially modulates rapidly inactivating and per-

sistent sodium currents in prefrontal cortex pyramidal neurons. J Neurosci 21, 2268–2277
29. Meisler MH, Sprunger LK, Plummer NW, Escayg A, Jones JM (1997) Ion channel mutations in mouse models of inherited neurological disease. Ann Med 29, 569–574
30. Meisler MH, Kearney J, Escayg A, MacDonald BT, Sprunger LK (2001a) Sodium channels and neurological disease: insights from *Scn8a* mutations in the mouse. Neuroscientist 7, 136–145
31. Meisler MH, Kearney J, Ottman R, Escayg A (2001b) Identification of epilepsy genes in human and mouse. Annu Rev Genet 35, 567–588
32. Mouse Genome Sequencing Consortium(2002) Initial sequencing and comparative analysis of the mouse genome. Nature 420, 520–562
33. Ohmori I, Ouchida M, Ohtsuka Y, Oka E, Shimizu K (2002) Significant correlation of the SCN1A mutations and severe myoclonic epilepsy in infancy. Biochem Biophys Res Commun 295, 17–23
34. Pittler SJ, Baehr W (1991) Identification of a nonsense mutation in the rod photoreceptor cGMP phosphodiesterase beta-subunit gene of the rd mouse. Proc Natl Acad Sci USA 88, 8322–8326
35. Raman IM, Sprunger LK, Meisler MH, Bean BP (1997) Altered subthreshold sodium currents and disrupted firing patterns in purkinje neurons of *Scn8a* mutant mice. Neuron 19, 881–891
36. Rinchik EM, Carpenter DA (1999) N-ethyl-N-nitrosourea mutagenesis of a 6- to 11-cM subregion of the Fah-Hbb interval of mouse chromosome 7: completed testing of 4557 gametes and deletion mapping and complementation analysis of 31 mutations. Genetics 152, 373–383
37. Schaller KL, Krzemien DM, Yarowsky PJ, Krueger BK, Caldwell JH (1995) A novel, abundant sodium channel expressed in neurons and glia. J Neurosci 15, 3231–3242
38. Sprunger LK, Escayg A, Tallaksen-Greene S, Albin RL, Meisler MH (1999) Dystonia associated with mutation of the neuronal sodium channel Scn8a and identification of the modifier loccus Scnm1 on mouse chromosome 3. Hum Mol Genet 8, 471–479
39. Sugawara T, Mazaki-Miyazaki E, Ito M, Nagafuji H, Fukuma G et al. (2001) $Na_v1.1$ mutations cause febrile seizures associated with agebrile partial seizures. Neurology 57, 703–705
40. Sugawara T, Tsurubuchi Y, Fujiwara T, Mazaki-Miyazaki E, Nagata K et al. (2003) $Na_v1.1$ channels with mutations of severe myoclonic epilepsy in infancy display attenuated currents. Epilepsy Res 54, 201–207
41. Thaung C, West K, Clark BJ, McKie L, Morgan JE et al. (2002) Novel ENU-induced eye mutations in the mouse: models for human eye disease. Hum Mol Genet 11, 755–767
42. Vreugde S, Erven A, Kros CJ, Marcotti W, Fuchs H et al. (2002) Beethoven, a mouse model for dominant, progressive hearing loss DFNA36. Nat Genet 30, 257–258
43. Williams RW, Flaherty L, Threadgill DW (2003) The math of making mutation mice. Genes Brain Behav 2, 191–200
44. Yamagishi T, Li RA, Hsu K, Marban E, Tomaselli GF (2001) Molecular architecture of the voltage-dependent Na channel: functional evidence for alpha helices in the pore. J Gen Physiol 118, 171–182
45. Yu FH, Catterall WA (2003) Overview of the voltage-gated sodium channel family. Genome Biol 4, 207